Aust. J. Phys., 1985, **38**, 191–208

Dynamics of a Nonlinear Diatomic Chain. III* A Molecular Dynamics Study

B. I. Henry[A,B] *and J. Oitmaa*[A]

[A] School of Physics, University of New South Wales,
P.O. Box 1, Kensington, N.S.W. 2033.
[B] Present address: Department of Physics,
University of Waterloo, Waterloo, Ontario, N2L 3G1, Canada.

Abstract

We investigate the dynamics and the statistical mechanics of a nonlinear diatomic model for a solid which may undergo a displacive structural phase transition (DSPT), using the molecular dynamics (MD) technique. Snapshots of the lattice displacement pattern reveal the presence of kinks at low temperatures. MD collision experiments show that the kinks exhibit soliton-like behaviour. Phonon wave packets are observed to pass through kinks and kinks and anti-kinks interact with one another with little distortion. The MD data are used to calculate the dynamical structure factor for the displacement fields in the diatomic chain. The dynamical structure factor is found to exhibit a central peak when the lattice displacement pattern is dominated by kinks. At small but finite wave vectors the central peak splits producing a new excitation branch in addition to the usual soft-mode phonon side-band. The central peak does not arise from self-consistent phonons but is dependent on the presence of kinks. The height of the peak increases and the width of the peak decreases as the temperature goes to zero.

1. Introduction

In previous work we have investigated the dynamics (Henry and Oitmaa 1983; referred to here as Part I) and the statistical mechanics (Henry and Oitmaa 1985; Part II, present issue p. 171) of a nonlinear diatomic model for a solid which may undergo a displacive structural phase transition (DSPT). The model is described by the Hamiltonian

$$H = \sum_{i=1}^{N} \tfrac{1}{2}M_1 \dot{u}_i^2 + \tfrac{1}{2}M_2 \dot{v}_i^2 + \tfrac{1}{2}\gamma(u_i - v_{i-1})^2 + \tfrac{1}{2}\gamma(u_i - v_i)^2 - \tfrac{1}{2}Au_i^2 + \tfrac{1}{4}Bu_i^4 , \quad (1)$$

where u_i and $\dot{u}_i$ (v_i and $\dot{v}_i$) are the displacement from equilibrium and the velocity respectively for atoms of mass M_1 (M_2) in the ith unit cell. This model extends a much studied model for solids undergoing a DSPT to include two species per unit cell. If the parameter γ which determines the coupling of the field is sufficiently large so that the intersite strain energy is larger than the depth of the potential wells, then a continuum approximation can be employed (Krumhansl and Schrieffer 1975).

* Part II, *Aust. J. Phys.*, 1985, **38**, 171–89.

0004-9506/85/020191$02.00

In this displacive regime the field equations yield topological kink solitons in addition to linearized phonons (Henry and Oitmaa 1983). In Part II we established that the kinks and phonons dominate the excitation spectrum for the lattice at low temperatures. The nonlinear vibrational excitations (kinks) were found to be responsible for a central peak in the dynamical structure factor.

In the present paper we examine the dynamics and the statistical mechanics for the diatomic ϕ^4 chain using the molecular dynamics (MD) technique. These computer simulations show the main physical features postulated in previous work for the behaviour of the displacement fields (Part I) and for the behaviour of the thermodynamic properties (Part II) of the lattice. The plan of this paper is as follows: In Section 2 we use computer experiments to examine interactions between phonon wave packets (both acoustic and optical) and kinks, and interactions between kinks and anti-kinks. These experiments demonstrate the important soliton-like behaviour of the kinks. In Section 3 we introduce a constant temperature MD procedure. This is then used to investigate the lattice displacement pattern at a number of temperatures and the temperature dependence of the kink density is studied in this way. In Section 4 the data generated from the constant temperature MD simulations are used to compute the dynamical structure factor for the lattice. A central peak is observed in the dynamical structure factor when the lattice displacement pattern is dominated by kinks. In Section 5 we present our conclusions.

2. Interactions between Excitations

Introducing the dimensionless quantities

$$\xi = u/u_0, \quad \eta = v/u_0, \quad \bar{\gamma} = \gamma/A, \quad \overline{m} = M_2/M_1, \quad \bar{t} = (A/M_1)^{\frac{1}{2}}t, \tag{2}$$

we can write the discrete lattice equations of motion for the model in the convenient computational form

$$\mathrm{d}^2\xi_n/\mathrm{d}\bar{t}^2 = -\xi_n^3 + (1-2\bar{\gamma})\xi_n + \bar{\gamma}(\eta_n + \eta_{n-1}), \tag{3a}$$

$$\overline{m}\,\mathrm{d}^2\eta_n/\mathrm{d}\bar{t}^2 = -2\bar{\gamma}\eta_n + \bar{\gamma}(\xi_{n+1} + \xi_n). \tag{3b}$$

In this section we employ the MD technique to investigate interactions between kinks and phonon wave packets and interactions between kinks and anti-kinks. Since the kinks studied in this section were obtained from a continuum limit description of the lattice (Part II) we choose $\bar{\gamma} \gg 1$ (the displacive regime) for which the continuum approximation is valid. For $\bar{\gamma} < 1$ discrete lattice effects become important; for example, in this regime kinks radiate phonons resulting in a damping of their motion (Henry 1984). The MD technique replaces the second derivatives in equations (3) by a difference algorithm with a time increment (Beeman 1976). The time increment was chosen in such a way that, by doubling the number of integration steps and halving the time increment, the final displacement pattern was not altered in any substantial way. A time increment of $h = 0{\cdot}01$ was found to be suitable. The MD run was started with $2N$ initial positions and velocities. The algorithm delivers the set of variables $\xi_n, \dot{\xi}_n, \eta_n, \dot{\eta}_n$ after each time step. The experiments described in this section were performed with $N = 200$ and the ends of the chain were left free.

Kink/Phonon Interactions

The phonons are represented by a gaussian wave packet of width Δ which is initially well separated from a static kink, and moves towards the kink with group velocity v_g. The dimensionless coupling has been chosen as $\bar{\gamma} = 16$. In this highly displacive regime discrete lattice effects should be negligible. The initial displacements and velocities are chosen to be

$$\xi_n(0) = \tanh\{(n-n_k)/\Delta_0\} + \alpha_1 \exp[-\{(n-n_p)/\Delta\}^2]\cos(q_0 n), \tag{4a}$$

$$\dot{\xi}_n(0) = (2v_g/\Delta)\alpha_1(n-n_p)\exp[-\{(n-n_p)/\Delta\}^2]\cos(q_0 n) + \alpha_1 \omega(q_0)\sin(q_0 n)\exp[-\{(n-n_p)/\Delta\}^2], \tag{4b}$$

$$\begin{aligned}\eta_n(0) = {} & (1-2/\Delta_0^2)\tanh\{(n-n_k)/\Delta_0\} + (2/\Delta_0^2)\tanh^3\{(n-n_k)/\Delta_0\} \\ & + (1/2\Delta_0)(1-2/\Delta_0^2)\operatorname{sech}^2\{(n-n_k)/\Delta_0\} \\ & + (3/\Delta_0^3)\tanh^2\{(n-n_k)/\Delta_0\}\operatorname{sech}^2\{(n-n_k)/\Delta_0\} \\ & - (1/4\Delta_0^2)(1-2/\Delta_0^2)\operatorname{sech}^2\{(n-n_k)/\Delta_0\}\tanh\{(n-n_k)/\Delta_0\} \\ & + (3/2\Delta_0^4)\tanh\{(n-n_k)/\Delta_0\}\operatorname{sech}^4\{(n-n_k)/\Delta_0\} \\ & - (3/2\Delta_0^4)\operatorname{sech}^2\{(n-n_k)/\Delta_0\}\tanh^3\{(n-n_k)/\Delta_0\} \\ & + \alpha_2 \exp[-\{(n+\tfrac{1}{2}-n_p)/\Delta\}^2]\cos\{q_0(n+\tfrac{1}{2})\},\end{aligned} \tag{4c}$$

$$\dot{\eta}_n(0) = (2v_g/\Delta)\alpha_2(n+\tfrac{1}{2}-n_p)\exp[-\{(n+\tfrac{1}{2}-n_p)/\Delta\}^2]\cos\{q_0(n+\tfrac{1}{2})\} + \alpha_2 \omega(q_0)\sin\{q_0(n+\tfrac{1}{2})\}\exp[-\{(n+\tfrac{1}{2}-n_p)/\Delta\}^2], \tag{4d}$$

with

$$\Delta_0 = \bar{\gamma}^{\frac{1}{4}}. \tag{4e}$$

The kink and the wave packet are initially located at the n_kth and n_pth particle respectively. The dispersion $\omega(q_0)$ of the harmonic excitations of the equations of motion (3) linearized about $\xi = \eta = \pm 1$ is given by

$$\bar{\omega}^2(\pm) = \{\bar{\gamma}(\bar{m}^{-1}+1)+1\}\left\{1 \pm \left(1 - \frac{4\bar{\gamma}(1+\bar{\gamma}\sin^2\frac{1}{2}q_0)}{\bar{m}\{\bar{\gamma}(\bar{m}^{-1}+1)+1\}^2}\right)^{\frac{1}{2}}\right\}, \tag{5}$$

where the plus sign corresponds to an optical mode and the minus sign corresponds to an acoustic mode (Henry 1984). The wave packet group velocity is given by

$$v_g(\pm) \equiv \left.\frac{d\bar{\omega}}{dq}\right|_{q_0} = \frac{\pm\bar{\gamma}^2\sin q_0}{\bar{m}\{\bar{\gamma}(\bar{m}^{-1}+1)+1\}}\frac{1}{\bar{\omega}}\left(1 - \frac{4\bar{\gamma}(1+\bar{\gamma}\sin^2\frac{1}{2}q_0)}{\bar{m}\{\bar{\gamma}(\bar{m}^{-1}+1)+1\}^2}\right)^{-\frac{1}{2}}, \tag{6}$$

where the minus sign now corresponds to the optical mode and the plus sign to the acoustic mode. In the following experiments the u-field wave packet amplitude is given by $\alpha_1 = 0{\cdot}25$. The v-field wave packet amplitude α_2 is then obtained from the ratio

$$\alpha_1/\alpha_2 = \{2\bar{\gamma} - \bar{m}\bar{\omega}^2(\pm)\}/2\bar{\gamma}\cos\tfrac{1}{2}q_0. \tag{7}$$

The wave packet width Δ and the wave vector q_0 have been set to 25 and $\frac{1}{5}\pi$ respectively.

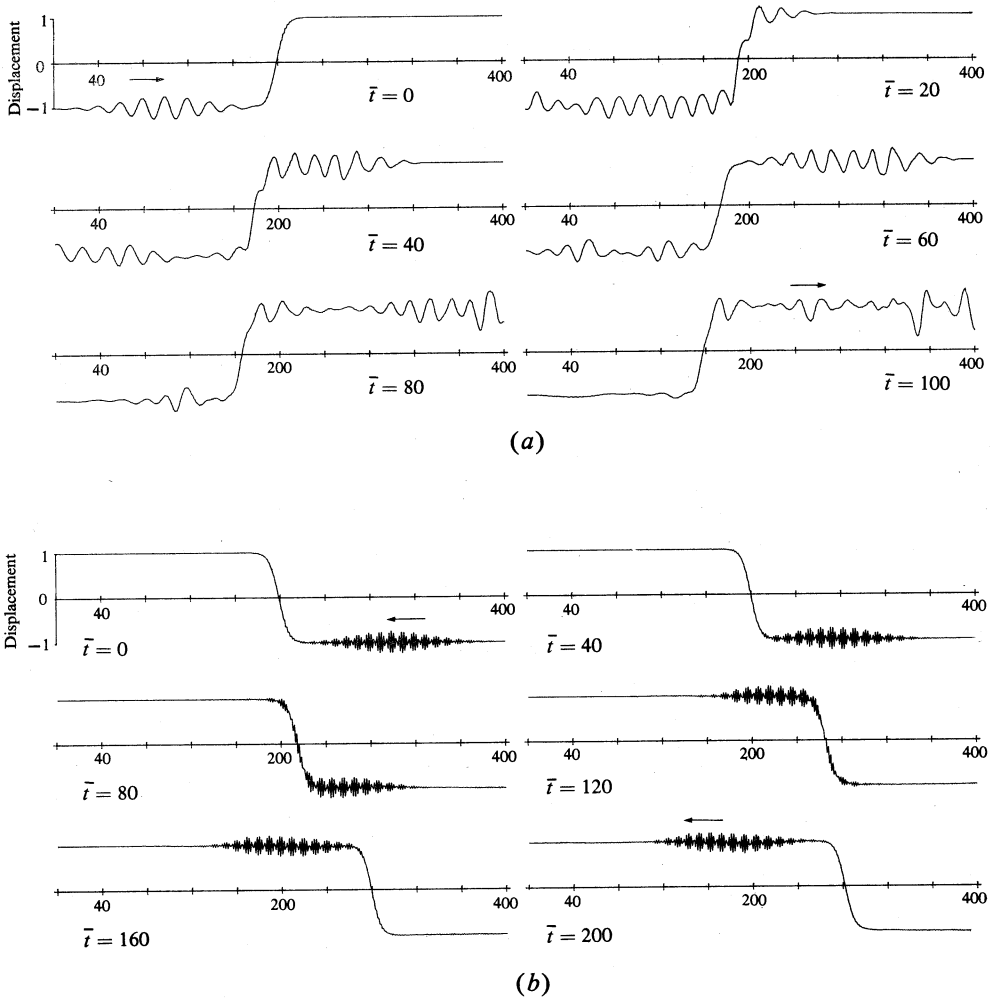

Fig. 1. Equal time snapshots of an MD experiment simulating the collision between a phonon wave packet and a static kink in the diatomic ϕ^4 chain: (*a*) snapshots at intervals of $\bar{t} = 20$ for an acoustic phonon; (*b*) snapshots at intervals of $\bar{t} = 40$ for an optical phonon. The wave vector in both cases is given by $q_0 = \frac{1}{3}\pi$, the coupling constant by $\bar{\gamma} = 16$ and the mass ratio by $\bar{m} = 1$.

Fig. 1*a* shows equal time snapshots of an acoustic phonon wave packet colliding with a static kink in the diatomic ϕ^4 chain with $\bar{m} = 1$. The snapshots represent the displacement pattern after intervals of 2000 integration steps. The acoustic wave packet is broken up by the kink. The kink is accelerated through the wave packet resulting in a shift in the kink position. The deformation of the wave packet is due in part to the different phase shifts of the modes building up the wave packet. Hasenfratz and Klein (1977) have investigated the interaction between a static kink and a phonon wave packet in the monatomic ϕ^4 chain. Their results are similar to those obtained here for the static kink/acoustic phonon interaction. Fig. 1*b* shows equal time snapshots of an optical phonon wave packet colliding with a static kink. In this experiment the snapshots represent the displacement pattern after 4000 steps.

Both the wave packet and the kink preserve their shape in this collision; however, the kink is shifted by the interaction. The kink is accelerated towards the increasing amplitude of the wave packet. When half of the wave packet has passed through the kink, the kink begins to decelerate until it finally comes to rest when the wave packet has passed completely through it.

Kink/Anti-kink Interactions

In the following MD experiments an equal-displacement-field kink propagating to the right is set up to collide with a similar anti-kink propagating to the left. The initial velocity of both the kink and the anti-kink, $\bar{c}_0 = (\bar{\gamma}/4\overline{m})^{\frac{1}{2}}$, is fixed by the parameters of the lattice. The initial lattice positions and velocities are given by

$$\xi_n(0) = \tanh\{(n-n_k)/\Delta_k\} - \tanh\{(m-n_{\bar{k}})/\Delta_k\}, \tag{8a}$$

$$\dot{\xi}_n(0) = -(\bar{c}_0/\Delta_k)\operatorname{sech}^2\{(n-n_k)/\Delta_k\} - (\bar{c}_0/\Delta_k)\operatorname{sech}^2\{(m-n_{\bar{k}})/\Delta_k\}, \tag{8b}$$

$$\begin{aligned}\eta_n(0) = {} & \tanh\{(n-n_k)/\Delta_k\} + (1/2\Delta_k)\operatorname{sech}^2\{(n-n_k)/\Delta_k\} \\ & - (1/4\Delta_k^2)\operatorname{sech}^2\{(n-n_k)/\Delta_k\}\tanh\{(n-n_k)/\Delta_k\} \\ & - \tanh\{(m-n_{\bar{k}})/\Delta_k\} - (1/2\Delta_k)\operatorname{sech}^2\{(m-n_{\bar{k}})/\Delta_k\} \\ & + (1/4\Delta_k^2)\operatorname{sech}^2\{(m-n_{\bar{k}})/\Delta_k\}\tanh\{(m-n_{\bar{k}})/\Delta_k\},\end{aligned} \tag{8c}$$

$$\begin{aligned}\dot{\eta}_n(0) = {} & -(\bar{c}_0/\Delta_k)\operatorname{sech}^2\{(n-n_k)/\Delta_k\} + (\bar{c}_0/\Delta_k^2)\operatorname{sech}^2\{(n-n_k)/\Delta_k\}\tanh^2\{(n-n_k)/\Delta_k\} \\ & - (\bar{c}_0/2\Delta_k^3)\operatorname{sech}^2\{(n-n_k)/\Delta_k\}\tanh^2\{(n-n_k)/\Delta_k\} + (\bar{c}_0/4\Delta_k^3)\operatorname{sech}^4\{(n-n_k)/\Delta_k\} \\ & - (\bar{c}_0/\Delta_k)\operatorname{sech}^2\{(m-n_{\bar{k}})/\Delta_k\} + (\bar{c}_0/\Delta_k^2)\operatorname{sech}^2\{(m-n_{\bar{k}})/\Delta_k\}\tanh^2\{(m-n_{\bar{k}})/\Delta_k\} \\ & - (\bar{c}_0/2\Delta_k^3)\operatorname{sech}^2\{(m-n_{\bar{k}})/\Delta_k\}\tanh\{(m-n_{\bar{k}})/\Delta_k\} + (\bar{c}_0/4\Delta_k^3)\operatorname{sech}^4\{(m-n_{\bar{k}})/\Delta_k\},\end{aligned} \tag{8d}$$

with

$$\Delta_k = \{\tfrac{1}{2}\gamma(1-\overline{m}^{-1})\}^{\frac{1}{2}}, \tag{8e}$$

where $n = 1, 2, ..., n_L$ and $m = n_L, n_{L+1}, ..., N$. The kink and the anti-kink are initially located at the n_k th and $n_{\bar{k}}$ th site respectively.

The domain wall MD collision experiments we have performed show that the usual soliton properties are obeyed, i.e. the kink and the anti-kink reflect each other. However, in contrast to the N soliton solutions of the sine–Gordon and $K\,dV$ equations (see e.g. Scott *et al.* 1973), the domain walls of our model dissipate part of their kinetic energy in the form of radiation (phonon) energy.

In the monatomic ϕ^4 chain, the outcome of domain wall MD collision experiments depends critically upon the initial domain wall velocities. For high velocities $c \gtrsim 0{\cdot}5c_A$ (where c_A is the lattice sound velocity) the domain walls reflect each other, whereas for low velocities $c < 0{\cdot}5c_A$ the domain walls annihilate each other upon collision. Furthermore, channels of annihilation have been found in which walls annihilate for $c = c_0$, but do not for $c = c_0 \pm \varepsilon$ (Aubry 1976). In the diatomic ϕ^4 chain, however, we have observed the soliton properties of domain walls reflecting each other for all velocities chosen in the range $0{\cdot}1 < \bar{c} < 0{\cdot}9$. Equal time snapshots of a typical domain wall MD collision experiment are shown in Fig. 2.

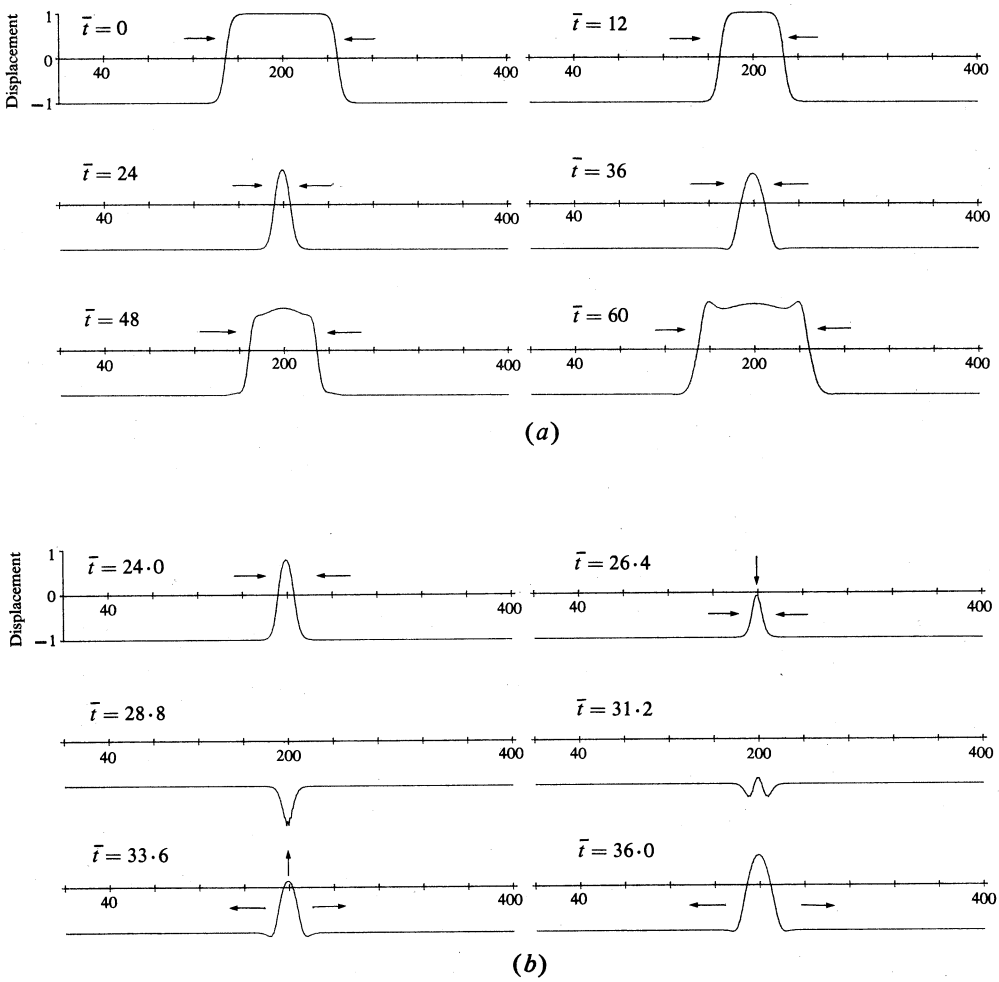

Fig. 2. Equal time snapshots of an MD experiment simulating the collision between an equal-displacement-field kink and anti-kink in the diatomic ϕ^4 chain: (*a*) snapshots at intervals of $\bar{t} = 12$; (*b*) snapshots at intervals of $\bar{t} = 2{\cdot}4$, showing details of the domain walls passing through one another. The coupling constant is $\bar{\gamma} = 16$ and the mass ratio $\bar{m} = 5$.

The computer experiments reported in this section show that kinks and anti-kinks (domain walls) enjoy quasi-soliton properties, behaving in many respects like deformable particles. Acoustic phonon wave packets are partially reflected and partially transmitted by kinks, whereas optical phonon wave packets are completely transmitted by the kinks. The kinks are spatially shifted by the incident phonon wave packets. As a final example in this context, domain walls are reflected by collisions with other domain walls without annihilation dissipating some of their kinetic energy as radiation energy.

3. Lattice Configurations in Thermal Equilibrium

In this section we employ a constant temperature MD procedure to investigate the lattice displacement pattern for the diatomic ϕ^4 chain, when the system is in thermal equilibrium.

The MD simulation is started with the initial positions and velocities of the particles in the chain chosen to represent a typical low-temperature low-energy configuration. The lattice displacements $u_n(jh)$ and velocities $\dot{u}_n(jh)$ of the $n = 0, 1, ..., N-1$ particles at times jh ($j = 0, ..., M-1$; h is the integration step size) are then obtained by employing an integrating algorithm. The time history of each particle after a run is called the sample function for the data. The total data consist of an ensemble of sample functions. The zero of time in an MD run is set after a large number of integrations are performed in order to eliminate initial bias. If the temperature is kept constant, then the average of the particle displacements will be essentially constant in time, i.e.

$$\bar{u}(0) = \bar{u}(h) = \ldots \bar{u}((M-1)h), \tag{9}$$

where

$$\bar{u}(jh) = \frac{1}{N}\sum_{k=1}^{N} u_k(jh). \tag{10}$$

The random data obtained from these MD simulations are therefore stationary and ergodic. This means that time averages can be used for ensemble averages (Bendat and Piersol 1966). For example, the average displacement of any particular particle k can be computed using a time average, namely

$$\langle u_k \rangle = \frac{1}{T}\int_0^T u_k(t)\,\mathrm{d}t = \frac{h}{M}\sum_{j=0}^{M-1} u_k(jh).$$

The dimensionless temperature of the diatomic ϕ^4 chain $\bar{T} = k_B TBA^{-2}$ is calculated using

$$\bar{T} = \tfrac{1}{2}\langle \bar{\dot{\xi}}^2 + \bar{m}\bar{\dot{\eta}}^2 \rangle, \tag{11}$$

where $\bar{\dot{\xi}}^2$ and $\bar{\dot{\eta}}^2$ are the mean square velocities of the M_1 and M_2 atoms respectively. The angle brackets denote the ensemble average which is evaluated as the time average over a run. In order to have a useful temperature control whilst maintaining stability, we have employed a predictor/corrector algorithm developed by Beeman (1976). This algorithm includes the velocities $\dot{r}_n(t)$ in the predictor used to calculate the positions $r_n(t+h)$ so that the temperature of the system may be adjusted by rescaling the velocities of the particles after a time step. The algorithm is described by the following equations:

$$P(r) = r_n(t+h) = r_n(t) + h\dot{r}_n(t) + \tfrac{1}{6}h^2\{4\ddot{r}_n(t) - \ddot{r}_n(t-h)\}, \tag{12a}$$

$$C(r) = r_n(t+h) = r_n(t) + h\dot{r}_n(t) + \tfrac{1}{6}h^2\{\ddot{r}_n(t+h) - 2\ddot{r}_n(t)\}, \tag{12b}$$

$$C(\dot{r}) = \dot{r}_n(t+h) = h^{-1}\{r_n(t+h) - r_n(t)\} + \tfrac{1}{6}h^2\{2\ddot{r}_n(t+h) + \ddot{r}_n(t)\}. \tag{12c}$$

Beeman showed that this algorithm was both stable and energy conserving when applied in the sequence $P(r) \to \ddot{r}_n \to C(r) \to \ddot{r}_n \to C(\dot{r})$. The temperature of the system was held constant by employing the following scheme. The initial velocities were chosen as

$$\dot{\xi}_n(0) = \bar{T}_0^{\frac{1}{2}}, \qquad \dot{\eta}_n(0) = (\bar{T}_0/\bar{m})^{\frac{1}{2}}. \tag{13a, b}$$

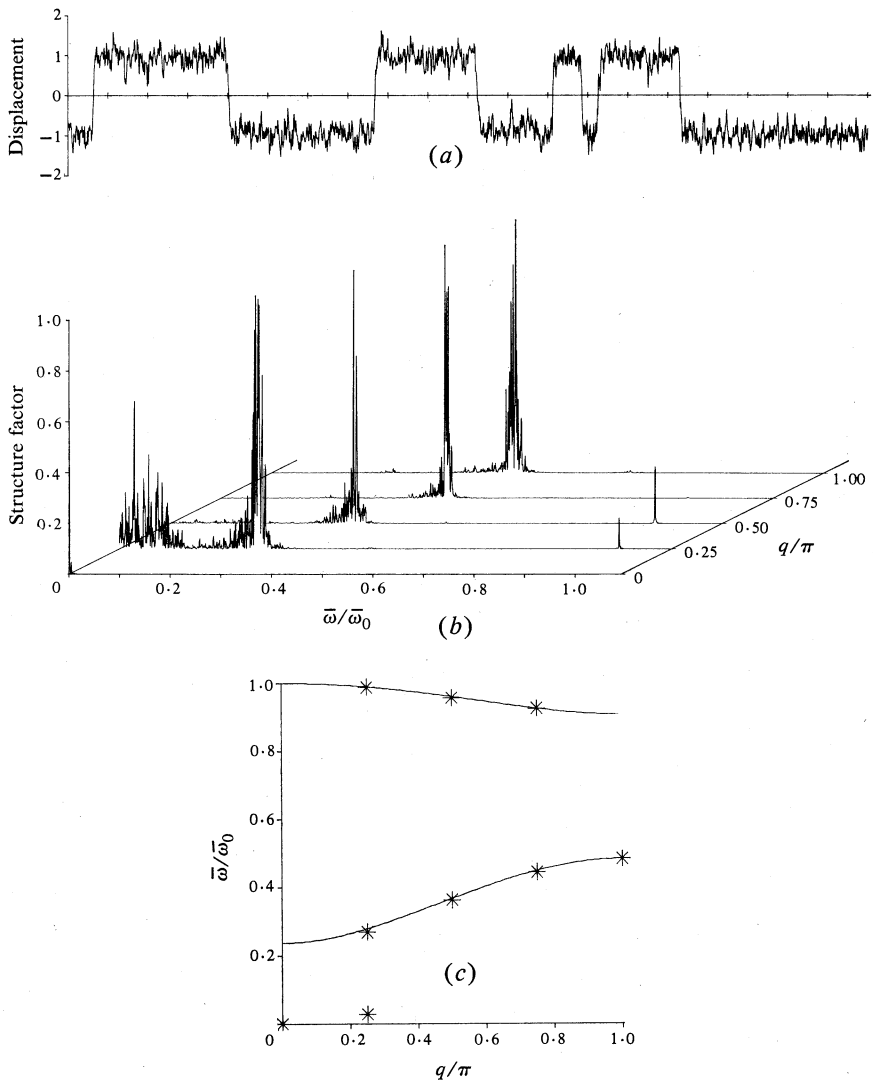

Fig. 3. Results from a constant temperature MD simulation of a periodic nonlinear diatomic chain consisting of 2000 harmonically coupled particles M_1 and M_2, including a nonlinear potential on the M_1 species. The coupling constant was set to $\bar{\gamma} = 2$ and the mass ratio $\bar{m} = 0{\cdot}2$. The run was performed for 2^{14} steps after the zero of time, using a step size of $h = 0{\cdot}05$. The temperature is $\bar{T} = 0{\cdot}1$. (*a*) Snapshots of the lattice displacement pattern at $\bar{t} = 2^{14}h$. (*b*) The dynamical structure factor $S(q, \bar{\omega})/S(q, \bar{\omega}_0)$ for the displacement field of the M species at the five wave vectors $q = 0$, $\frac{1}{4}\pi$, $\frac{1}{2}\pi$, $\frac{3}{4}\pi$ and π. (*c*) The dispersion law obtained from the positions of the peaks in the structure factor (*stars*) and the SCPA dispersion law (equation A9) for the nonlinear diatomic chain (*curves*).

Thus, the initial temperature is given by $\bar{T}(0) = \bar{T}_0$. The velocities were then rescaled after each time step according to

$$\tilde{\dot{\xi}}_n(t) = s(t)\dot{\xi}_n(t), \qquad \tilde{\dot{\eta}}_n(t) = s(t)\dot{\eta}_n(t), \tag{14a, b}$$

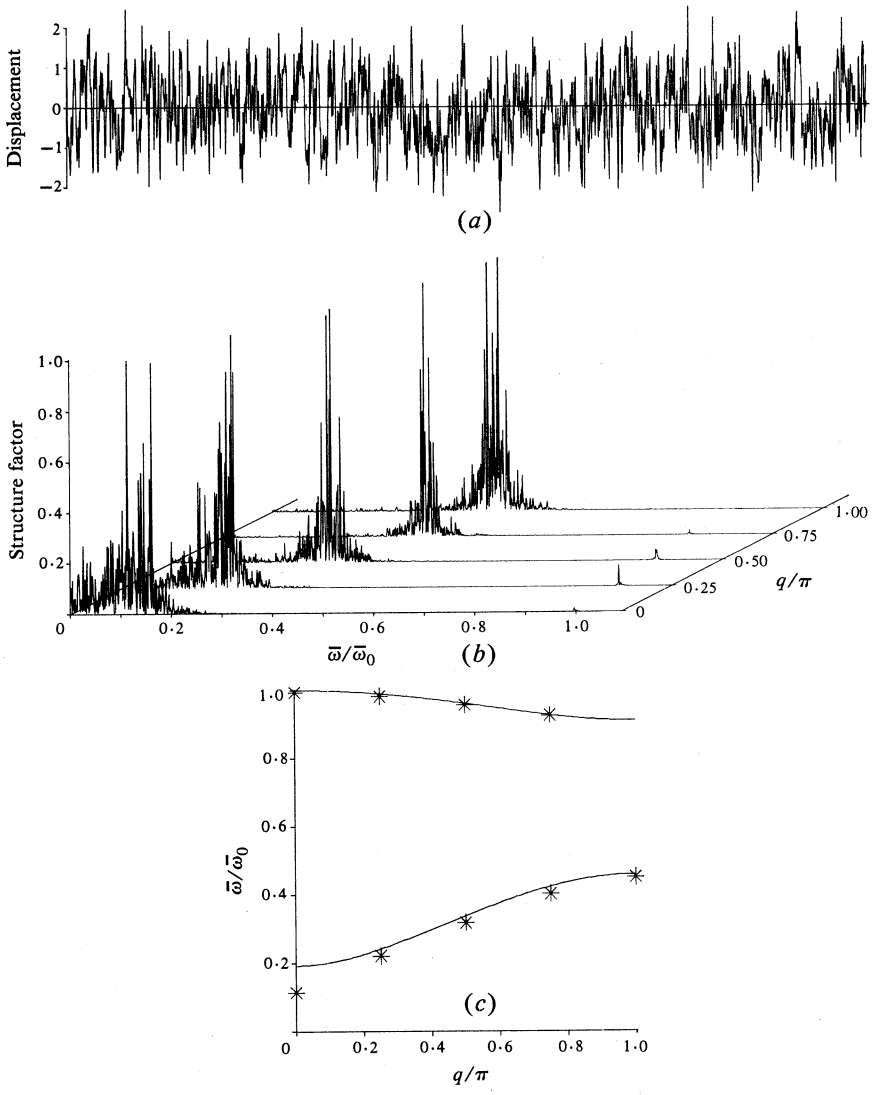

Fig. 4. As for Fig. 3, except the temperature of the lattice is $\bar{T} = 0{\cdot}5$.

where the scale factor $s(t)$ is evaluated after each time step as follows:

$$s(t) = \bar{T}_0^{\frac{1}{2}} \left\{ \tfrac{1}{2} \left(\frac{1}{N} \sum_{i=0}^{N-1} \dot{\xi}_i^2(t) + \frac{\bar{m}}{N} \sum_{i=0}^{N-1} \dot{\eta}_i^2(t) \right) \right\}^{-\frac{1}{2}} . \tag{15}$$

This rescales the temperature $\bar{T}(t)$ after each time step to the constant temperature $\bar{T}_0$.

The stability of the Beeman algorithm for integrating the equations of motion describing the nonlinear diatomic chain was investigated by observing changes in the lattice displacement pattern with changes in the integration step size. We found that a step size of $h = 0{\cdot}05$ was sufficient to ensure stability.

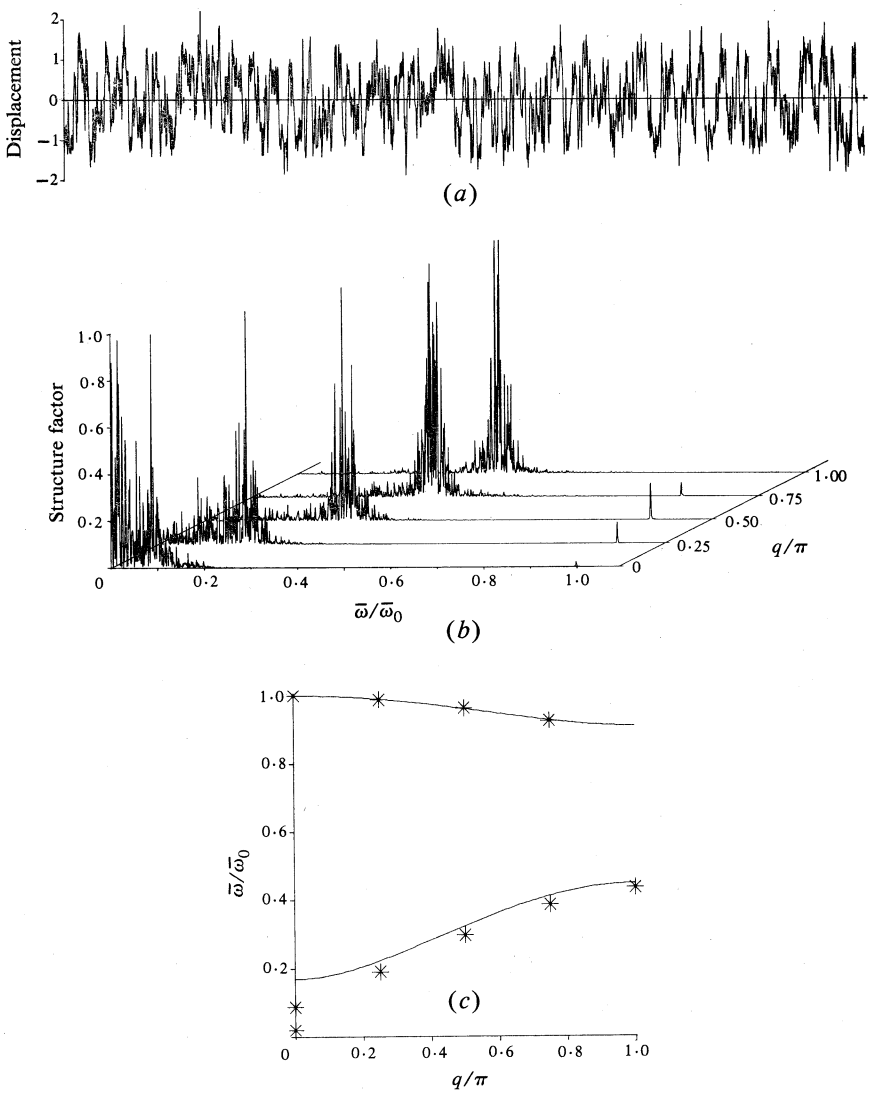

Fig. 5. As for Fig. 3, except the temperature of the lattice is $\bar{T} = 1{\cdot}0$.

We have performed a constant temperature MD simulation of the nonlinear diatomic chain using a step size of $h = 0{\cdot}05$ for a system of 2000 particles (1000 unit cells) subject to periodic boundary conditions. The MD run was initiated with the particles randomly displaced a small distance from the ground state configuration $\xi = \eta = -1$. The zero of time was set after 10000 integration steps in order to eliminate initial bias. In the runs reported here the coupling constant was set to $\bar{\gamma} = 2$, which is in the displacive regime, and the mass ratio was set to $\bar{m} = 0{\cdot}2$.

Figs 3*a*, 4*a* and 5*a* show snapshots of the lattice displacement pattern at $\bar{t} = 2^{14}h$ for the three temperatures $\bar{T} = 0{\cdot}1$, $0{\cdot}5$ and $1{\cdot}0$. The temperature control in the present MD simulation enables us to investigate the temperature dependence of the

domain wall concentration. The domain wall density is given analytically by (see Part II)

$$\bar{n}_K \approx \bar{T}^{-\frac{1}{2}} \exp(-\bar{E}_K^0/\bar{T}), \tag{16}$$

where the dimensionless kink energy is

$$\bar{E}_K^0 = \tfrac{2}{3}\gamma^{\frac{1}{2}}. \tag{17}$$

Equation (16) predicts densities of ~ 3 walls per 10^4 unit cells and ~ 200 walls per 10^3 unit cells for the respective temperatures $\bar{T} = 0{\cdot}1$ and $0{\cdot}5$. The MD results indicate ~ 5 walls per 10^3 unit cells and ~ 200 walls per 10^3 unit cells at these two temperatures. At the higher temperatures $\bar{T} \gtrsim 1{\cdot}0$ the domain walls have disappeared completely.

Koehler *et al.* (1975) have reported similar results from an MD simulation of the monatomic ϕ^4 chain. They suggested that the discrepancy between the computer results and theory for the kink density at low temperatures is due to interactions between kinks and phonons which would lead to an effective renormalization of the kink energy in equation (16). Phonon dressing of the domain walls can be seen in the MD snapshots.

Although the results reported here are for one mass ratio only, we have performed constant temperature MD simulations for three mass ratios such that $\bar{m} < 1$, $\bar{m} = 1$ and $\bar{m} > 1$. These simulations (Henry 1984) show the presence of domain walls for all three mass ratios at low temperatures.

The important conclusions to be made from the MD snapshots of the lattice configurations in the nonlinear diatomic chain may be summarized as follows:

(i) The lattice displacement pattern is insensitive to changes in the mass ratio.

(ii) At low temperatures the lattice displacement pattern consists of phonon dressed domain walls.

(iii) The domain walls are destroyed by thermal fluctuations at temperatures above the static kink excitation energy.

(iv) The concentration of domain walls depends on the phonon dressing and requires the use of a renormalized kink energy in equation (16).

4. Dynamical Structure Factor

The leading approximation to the dynamical structure factor $S(q, \omega)$ is the space–time Fourier transform of the displacement–displacement correlation function

$$S(q,\omega) = \frac{1}{N}\int_{-\infty}^{+\infty} \exp(-\mathrm{i}\omega t) \sum_{n=0}^{N-1} \exp(-\mathrm{i}qn)\langle u_n(t)\, u_0(0)\rangle \, \mathrm{d}t, \tag{18}$$

where the wave vector is

$$q = 2\pi k/N; \qquad k = 0, 1, ..., N-1. \tag{19}$$

Following other workers (Bennett *et al.* 1982; Bishop *et al.* 1983) we compute the dynamical structure factor for the displacement fields in our chain as the squared modulus of the Fourier transform of the dynamical variable

$$X_q(t) = \frac{1}{N}\sum_{n=0}^{N-1} u_n(t) \exp(-\mathrm{i}qn). \tag{20}$$

An alternative approach is to proceed via the intermediate step of evaluating the correlation functions (Morf and Stoll 1977). The advantage of the former approach is that the dynamical variable $X_q(t)$ may be computed directly as the system evolves in the MD run. We compute the dynamical structure factor for the displacement fields using the following equations (for an explicit proof see Henry 1984):

$$S(q,\omega) \equiv S_k(l) = \lim_{M\to\infty} 2Mh\,|X_k(l)|^2, \tag{21}$$

where

$$X_k(l) = \frac{1}{2M}\sum_{l'=0}^{2M-1} X_q(l')\exp\{-\mathrm{i}\,\pi(l-l')/M\}, \tag{22}$$

with

$$X_q(l') = \frac{1}{N}\sum_{n=0}^{N} u_n(l'h)\exp(-\mathrm{i}\,qn). \tag{23}$$

The continuous frequency ω has been discretized according to

$$\omega = 2\pi l/2Mh; \qquad l = 0, 1, ..., 2M-1. \tag{24}$$

The dynamical variable $X_q(t)$ (defined by equation 23) is evaluated after each time step (i.e. as the system evolves). At the end of the run the discrete Fourier transform of the dynamical variable is computed as in equation (22). The dynamical structure factor is then evaluated using the square modulus of $X_k(l)$ in equation (21). The accuracy of the method may be improved by increasing the length of the MD run to approach $M \to \infty$ in equation (21).

In order to test the accuracy of the numerical procedure described above, we have applied it in Appendix 1 to calculate the dynamical structure factor for a diatomic chain including only harmonic interactions between nearest neighbours. The frequencies at which the dynamical structure factor exhibits peaks were then plotted against the wave vector. The dispersion law thus obtained was then compared with the well-known dispersion law for the harmonic diatomic chain. The excellent agreement between the two confirms the suitability of our numerical procedure.

Figs 3*b*, 4*b* and 5*b* show plots of the dynamical structure factor for the *u*-field displacements in the nonlinear diatomic chain at the five wave vectors $q = 0$, $\frac{1}{4}\pi$, $\frac{1}{2}\pi$, $\frac{3}{4}\pi$ and π. The dynamical variable $X_q(t)$ was computed from MD simulations of a system of 2000 particles subject to periodic boundary conditions. The zero of time was set after 10 000 steps in these simulations. The dynamical variable was evaluated at 2^{14} subsequent time steps. The Fourier transform of the dynamical variable was then obtained using a standard fast Fourier transform routine (Elliot and Rao 1982). The parameters $\bar{\gamma}$, $\bar{T}$ and $\bar{m}$ are the same as those in the accompanying plots (Figs 3*a*, 4*a* and 5*a*) of the lattice displacement pattern. The dynamical structure factor has been normalized to unity in these plots. The normalization used and the other relevant parameters from the MD run are recorded in Table 1. The fine structure of the peaks is due to noise in the numerical procedure. Although the statistical reliability of our numerical procedure may be improved by increasing the time span of the run ($M \to \infty$) the noise cannot be decreased in this way. In order to eliminate noise in the numerical procedure, it is necessary to introduce some sort of smoothing

technique. One possibility, equivalent to introducing gaussian demapping factors in space and time, is to average over neighbouring frequencies and wave vectors (Koehler and Lee 1976). We have not pursued this course here as we believe that the peaks in the dynamical structure factor are sufficiently resolved to yield physically meaningful results.

Table 1. Normalization used in the plots of the dynamical structure factor and the dispersion law for the diatomic φ^4 chain (Figs 3–5)

The temperature $\bar{T}$, the mean square displacement $\langle \bar{\xi}^2 \rangle$, and the normalizing frequency $\bar{\omega}_0$ are also given

q	0	$\frac{1}{4}\pi$	$\frac{1}{2}\pi$	$\frac{3}{4}\pi$	π
	Fig. 3: $\bar{T} = 0{\cdot}1$, $\langle \bar{\xi}^2 \rangle = 0{\cdot}8912$, $\bar{\omega}_0 = 4{\cdot}9291$				
$\bar{\omega}^*$	0	1·3269	1·7871	2·1859	2·3815
$S^0(q, \bar{\omega}^*)$	9·07329	0·00099	0·00111	0·00115	0·00057
	Fig. 4: $\bar{T} = 0{\cdot}5$, $\langle \bar{\xi}^2 \rangle = 0{\cdot}6138$, $\bar{\omega}_0 = 4{\cdot}9137$				
$\bar{\omega}^*$	0·4295	0·9357	1·4611	1·8945	2·1399
$S^0(q, \bar{\omega}^*)$	0·04566	0·01076	0·00425	0·00173	0·00193
	Fig. 5: $\bar{T} = 1{\cdot}0$, $\langle \bar{\xi}^2 \rangle = 0{\cdot}6959$, $\bar{\omega}_0 = 4{\cdot}9182$				
$\bar{\omega}^*$	0·5599	1·0853	1·5608	1·9750	2·2128
$S^0(q, \bar{\omega}^*)$	0·02737	0·01171	0·00670	0·00809	0·00331

In Figs 3*c*, 4*c* and 5*c* the dispersion law obtained from the structure factor peaks is compared with the self-consistent phonon dispersion law for the nonlinear diatomic chain [equation (A9) of Appendix 2]. The mean square displacement used in the latter was obtained from the MD simulations described above and is recorded in Table 1.

The main results obtained from these figures may be summarized as follows:

(i) At low temperatures (where the lattice displacement is dominated by kinks) and at zero wave vector, the dynamical structure factor for the u-field displacements exhibits a central peak around $\omega = 0$.

(ii) As the wave vector is increased at low temperatures the central peak splits into a double-peak structure giving rise to a new (kink manifested) excitation branch. The new branch does not persist above a critical wave vector q_c.

(iii) The intensity of the central peak decreases rapidly, and the width of the central peak increases rapidly, as the temperature is increased.

(iv) The self-consistent phonon approximation (SCPA) leads to a reasonable description of the phonon frequencies at all temperatures but fails to account for other nonlinear excitations.

(v) A soft-mode phonon occurs at a critical temperature $\bar{T}_0$ ($0{\cdot}5 < \bar{T} < 1{\cdot}0$) which is in the vicinity of the kink excitation energy.

The first three results have also been observed in MD simulations of the monatomic ϕ^4 chain (Schneider and Stoll 1976, 1981). The temperature dependence of the central peak is in qualitative agreement with the calculation of the kink contribution to the dynamical structure factor derived using an ideal gas phenomenology (see Part II). In this interpretation the narrowing of the central peak as $\bar{T} \to 0$ is a reflection of the time taken for a typical domain wall to diffuse over the distance of a growing cluster

length. The existence of a cut-off wave vector above which splitting of the central peak does not occur is due to all motions being harmonic above the critical wave vector (Aubry 1974)

$$q_c = \sqrt{2}\, a^{-1} \{ | V(u_0) | / \gamma u_0^2 \}^{\frac{1}{2}} .$$

The fourth result, whilst giving support for the SCPA theory in describing weakly nonlinear excitations, highlights the failure of SCPA theory to account for strongly nonlinear features such as the central peak. The fifth result is predicted by SCPA theory. The soft-mode temperature marks the temperature above which particles have sufficient energy to oscillate above the double-wall hump.

5. Conclusions

We have been studying the dynamics and the statistical mechanics of a nonlinear diatomic model for a solid which may undergo a displacive structural phase transition. In previous analytic studies (Parts I and II) we showed that in the displacive regime of the model Hamiltonian a continuum approximation is valid, in which case the equations of motion support nonlinear (kink) lattice excitations in addition to the usual linear (phonon) vibrations. Both types of mode behave as elementary excitations of the system at low temperatures. The low temperature thermodynamic properties can thus be computed from an ideal gas phenomenology incorporating the kinks and the phonons as quasi-particles. A prediction of this phenomenology is the existence of a central peak in the dynamical structure factor for the displacement field of the species in the double-wall potential.

In the present paper we have verified the analytic results using MD computer experiments. The intersite coupling was chosen to be representative of the displacive regime and the MD technique used to directly integrate the equations of motion. In the first of these experiments, the soliton-like behaviour of the kink solitary wave solutions to the coupled equations of motion was established. Phonon wave packets passed through kinks, and kinks and anti-kinks reflected from one another without significant distortion of the original kink profile. This particle like nature of the kinks is fundamental to their inclusion in ideal gas phenomenologies.

A study of the time evaluation of the particle displacements during an MD run shows two distinct features. The first is the rapid oscillation about a quasi-equilibrium position, together with the slow evolution of the quasi-equilibrium position itself. The second feature is the presence of well-defined domain walls in the lattice displacement pattern. The domain walls represent regions separating clusters of atoms in one quasi-equilibrium position from clusters in another quasi-equilibrium position. These domain walls correspond to the kink solitary waves derived from the continuum equations of motion. The density of the domain walls is observed to increase with increasing temperature, in qualitative agreement with the predictions of the kink density from the ideal gas phenomenology. Quantitative agreement is expected to depend on the inclusion of interactions between excitations in the phenomenology. Phonon dressing of the domain walls is observed in the MD simulations. At high temperatures the domain walls disappear completely, and the temperature at which this occurs is found to be close to the kink excitation energy. The two types of motion, rapid oscillations and slow evolution, are found to manifest themselves in the dynamical structure factor in the following way. The rapid oscillations give rise to a phonon side-band. The frequency of these oscillations decreases as the system

approaches a critical temperature above which all motions are oscillatory. The slow evolution of the quasi-equilibrium position leads to a peak centred about zero frequency in the dynamical structure factor. The height of this peak increases and the width decreases as the temperature goes to zero. This corresponds to the increasing size of the clusters observed in the displacement pattern as the temperature decreases. The existence of a central peak in the dynamical structure factor when the displacement pattern is dominated by kinks is in agreement with the prediction of ideal gas phenomenology of a kink dependent central peak.

Our results support the cluster picture (see Bruce and Cowley 1980, and references therein) for the central peak observed in the scattering cross section for inelastic neutron scattering experiments performed on $SrTiO_3$ (Shapiro *et al.* 1972). It should be pointed out, however, that our model is one-dimensional and therefore only undergoes a phase transition in a limited sense at $T = 0$ (the temperature at which the domain wall density also goes to zero). Cluster dynamics will certainly be important in three-dimensional systems, and the MD technique is likely to prove most useful for studying these systems. Some work has been done in this regard (Schneider and Stoll 1978), however, a more complete analysis is an important program for future research.

Acknowledgment

One of the authors (B.I.H.) would like to acknowledge support from a Commonwealth Postgraduate Research Award and from a Postgraduate Scholarship in Theoretical Physics from the Gordon Godfrey Bequest.

References

Aubry, S. (1974). *J. Chem. Phys.* **62**, 3217.
Aubry, S. (1976). *J. Chem. Phys.* **64**, 3392.
Beeman, D. (1976). *J. Comput. Phys.* **20**, 130.
Bendat, J. S., and Piersol, A. G. (1966). 'Measurement and Analysis of Random Data' (Wiley: New York).
Bennett, D., Bishop, A. R., and Trullinger, S. E. (1982). *Z. Phys.* B **47**, 265.
Bishop, A. R., Fesser, K., Lomdahl, P. S., Kerr, W. C., Williams, N. B., and Trullinger, S. E. (1983). *Phys. Rev. Lett.* **50**, 1095.
Bottger, H. (1983). 'Principles of Lattice Dynamics', p. 172 (Physik Verlag: Weinheim).
Bruce, A. D., and Cowley, R. C. (1980). *Adv. Phys.* **29**, 219.
Elliot, D. F., and Rao, K. R. (1982). 'Fast Transforms, Algorithms, Analyses, Applications' (Academic: New York).
Hasenfratz, W., and Klein, R. (1977). *Physica* A **89**, 191.
Henry, B. I. (1984). Ph.D. Thesis, Univ. New South Wales.
Henry, B. I., and Oitmaa, J. (1983). *Aust. J. Phys.* **36**, 339.
Henry, B. I., and Oitmaa, J. (1985). *Aust. J. Phys.* **38**, 171.
Koehler, T. R., Bishop, A. R., Krumhansl, J. R., and Schrieffer, J. A. (1975). *Sol. State Commun.* **17**, 1515.
Koehler, T. R., and Lee, P. A. (1976). *J. Comput. Phys.* **22**, 319.
Krumhansl, J. A., and Schrieffer, J. R. (1975). *Phys. Rev.* B **11**, 3535.
Morf, R. H., and Stoll, E. P. (1977). *In* 'Int. Series of Numerical Mathematics', Vol. 37 (Eds J. Descloux and J. Marti), p. 147 (Birkhauser: Basel).
Schneider, T., and Stoll, E. (1976). *Phys. Rev.* B **13**, 1216.
Schneider, T., and Stoll, E. (1978). *Phys. Rev.* B **17**, 1302.
Schneider, T., and Stoll, E. (1981). *Phys. Rev.* B **23**, 4631.
Scott, A. C., Chu, F. Y. F., and McLaughlin, D. W. (1973). *Proc. IEEE* **61**, 1443.
Shapiro, S. M., Axe, J. D., Shirane, G., and Riste, T. (1972). *Phys. Rev.* B **6**, 4332.

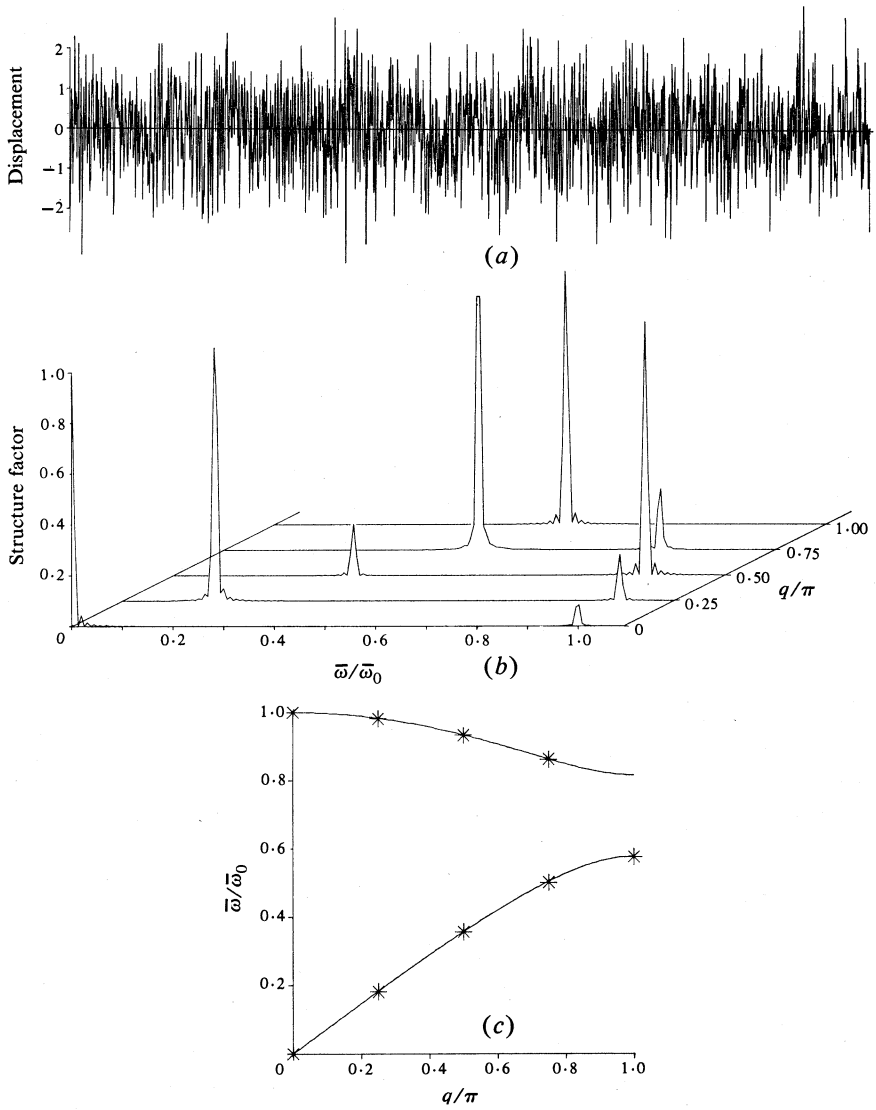

Fig. 6. Results from a constant temperature MD simulation of a periodic diatomic chain consisting of 2000 harmonically coupled particles M_1 and M_2. The coupling constant was set to $\bar{\gamma} = 1$, the mass ratio to $\bar{m} = 0{\cdot}5$ and the temperature to $\bar{T} = 1{\cdot}0$. The run was performed for 2^{12} steps after the zero of time, using a step size of $h = 0{\cdot}05$. (*a*) Snapshots of the lattice displacement pattern at $\bar{t} = 2^{12}h$. (*b*) The dynamical structure factor $S(q,\bar{\omega})/S(q,\bar{\omega}_0)$ for the displacement field of the M species at the five wave vectors $q = 0$, $\frac{1}{4}\pi$, $\frac{1}{2}\pi$, $\frac{3}{4}\pi$ and π. (*c*) The dispersion law obtained from the positions of the peaks in the structure factor (*stars*) and the dispersion law (equation A4) for the harmonic diatomic chain (*curves*).

Table 2. Normalization used in the plots of the dynamical structure factor and the dispersion law for the harmonic diatomic chain (Fig. 6)

The temperature, the mean square displacement and the normalizing frequency are given by $\bar{T} = 1{\cdot}0$, $\langle \zeta^{2} \rangle = 0{\cdot}9117$ and $\bar{\omega}_0 = 2{\cdot}4495$

q	0	$\frac{1}{4}\pi$	$\frac{1}{2}\pi$	$\frac{3}{4}\pi$	π
$\bar{\omega}^*$	0	0·4448	2·2856	1·2272	1·4113
$S^0(q,\bar{\omega}^*)$	0·008519	0·053875	0·005937	0·009175	0·005289

Appendix 1: Test of Numerical Procedure for Dynamical Structure Factor

In order to test the suitability of the numerical procedure outlined in Section 4 for evaluating the dynamical structure factor for the displacement fields, we consider the harmonic diatomic chain described by

$$H = \sum_{i=1}^{N} \tfrac{1}{2}M_1 \dot{u}_i^2 + \tfrac{1}{2}M_2 \dot{v}_i^2 + \tfrac{1}{2}\gamma(u_i - v_i)^2 + \tfrac{1}{2}\gamma(v_i - u_{i+1})^2 . \tag{A1}$$

The corresponding equations of motion are given by

$$M_1 \ddot{u}_n = -\gamma(2u_n - v_{n-1} - v_n), \qquad M_2 \ddot{v}_n = -\gamma(2v_n - u_n - u_{n+1}). \tag{A2a, b}$$

Introducing the dimensionless quantities

$$\bar{\gamma} = \gamma/A, \qquad \bar{m} = M_2/M_1, \qquad \bar{\omega} = (M_1/A)^{\frac{1}{2}}\omega, \tag{A3}$$

we obtain for the normal mode frequencies

$$\bar{\omega}^2(\pm) = \bar{\gamma}(\bar{m}+1)\left\{1 \pm \left(1 - \frac{4\bar{m}\sin^2\frac{1}{2}q}{(1+\bar{m})^2}\right)^{\frac{1}{2}}\right\}, \tag{A4}$$

where the lower branch $(-)$ is an acoustic mode and the upper branch $(+)$ an optical mode.

We have performed a constant temperature MD simulation of the harmonic diatomic chain using a step size of $h = 0{\cdot}05$ for a system of 2000 particles, subject to periodic boundary conditions. The temperature, coupling and mass ratio were set to $\bar{T} = 1$, $\bar{\gamma} = 1$ and $\bar{m} = 0{\cdot}5$ respectively. The zero of time $\bar{t} = 0$ was set after 5000 integration steps. The dynamical variable was then evaluated at 2^{12} subsequent time steps. Fig. 6*a* shows the lattice displacement pattern at $\bar{t} = 2^{12}h$, while Fig. 6*b* shows the dynamical structure factor at the five wave vectors $q = 0$, $\frac{1}{4}\pi$, $\frac{1}{2}\pi$, $\frac{3}{4}\pi$ and π. The dynamical structure factor has been normalized to unity in these plots. The normalization used is recorded in Table 2. Fig. 6*c* compares the dispersion law obtained from the structure factor peaks with the dispersion law for the harmonic diatomic chain (equation A4).

Appendix 2: Self-consistent Phonon Approximation

Here the optimal harmonic representation of the lattice is obtained using the self-consistent phonon approximation. The SCPA (also called the renormalized harmonic approximation) replaces the potential of a single atom by a renormalized potential which includes the effective potential arising from the motions of the surrounding atoms. The atomic motion is now governed by renormalized force constants rather than the bare force constants. The bare force constants are the equilibrium value of the second derivative of the potential. The renormalized force constants are the thermal average of the second derivatives of the potential (see e.g. Bottger 1983). In the present model (equation 1) the SCPA replaces the nonlinear potential by a harmonic potential according to

$$V(u_n) = \tfrac{1}{2}(-A + \tfrac{1}{2}B\langle u^2\rangle)u_n^2 = \tfrac{1}{2}A^*(T - T_0)u_n^2, \tag{A5}$$

where T_0 is the temperature above which all oscillations are harmonic (i.e. the temperature at which the in-wall oscillations are destroyed by thermal fluctuations). The quantity $\langle u^2 \rangle$ is to be evaluated using the thermal average

$$\langle u^2 \rangle = \int \mathrm{d}u\, u^2 \exp(-\beta H) \Big/ \int \mathrm{d}u \exp(-\beta H), \tag{A6}$$

where the Hamiltonian includes the renormalized potential (A5).

In the discrete lattice equations (3) the SCPA replaces the nonlinear term by a linear term as follows:

$$B\xi_n^3 = 3B\langle \xi^2 \rangle \xi_n. \tag{A7}$$

The self-consistent phonons are then given by

$$\xi_n = \xi_s \sin(qn - \omega t), \qquad \eta_n = \eta_s \sin\{q(n+\tfrac{1}{2}) - \omega t\}, \tag{A8a, b}$$

with dispersion

$$\bar{\omega}^2(\pm) = \{\bar{\gamma}(\bar{m}^{-1}+1) - \tfrac{1}{2} + \tfrac{3}{2}\langle \xi^2 \rangle\} \times \left\{1 \pm \left(1 - \frac{4\bar{m}^{-1}(6\bar{\gamma}^{-1}\langle \xi^2 \rangle - 2\bar{\gamma}^{-1} + 4\sin^2 \tfrac{1}{2}q)}{\{2(\bar{m}^{-1}+1) + 3\bar{\gamma}^{-1}\langle \xi^2 \rangle - \bar{\gamma}^{-1}\}^2}\right)^{\frac{1}{2}}\right\}. \tag{A9}$$

The lower branch $\omega^2(-)$ of (A9) is a quasi-acoustic mode and the upper branch $\omega^2(+)$ a quasi-optical mode.

Manuscript received 10 September 1984, accepted 8 January 1985